Prediction of electronic and optical properties for $Zn_{1-x}Cd_xSe_yTe_{1-y}$ quaternary alloys: First-principles study

K. Benchikh[a,*], M. Benchehima[a,b], H. Abid[a], and A. C. Chaouche[a]

[a]*Applied Materials Laboratory, Djillali Liabes University, Sidi Bel Abbes 22000, Algeria.*

[*]*e-mail: k_benchikh2002@yahoo.fr*

[b]*Electronic Department, University of Sciences and Technology of Oran, Mohamed Boudiaf (USTO), El M'nouar BP 1505, Oran, Algeria.*

Received 7 January 2021; accepted 28 January 2021

In the present work, the density functional theory (DFT) was performed for the investigation of the structural, electronic, and optical properties of the $Zn_{1-x}Cd_xSe_yTe_{1-y}$ quaternary alloys using the full potential linearized augmented plane wave (FP-LAPW) method. For the calculations of the structural properties, we have used the Perdew-Burke-Ernzerhof generalized gradient approximation (GGA-PBEsol). On the other hand, the electronic properties have been computed within the local density approximation (LDA) in addition to the Tran-Blaha modified Becke-Johnson (TB-mBJ) approach. Our results indicate that the lattice constant, as well as the bulk modulus and the energy gap for the $Zn_{1-x}Cd_xSe_yTe_{1-y}$ quaternary show almost linear variations on the concentration x ($0.125 \leq x \leq 0.875$). In addition, the simulated band structures for the $Zn_{1-x}Cd_xSe_yTe_{1-y}$ quaternary exhibit a direct-gap for all concentrations. Moreover, low bowing parameters are observed. Also, some interesting optical properties such as dielectric constant, refractive index, extinction coefficient, absorption coefficient, and reflectivity have been calculated by using the TB-mBJ method. The results of our computations show that the $Zn_{1-x}Cd_xSe_yTe_{1-y}$ quaternary alloy is a promising candidate for optoelectronic applications.

Keywords: Quaternary alloys; optical properties; density functional theory; TB-mBJ.

DOI: https://doi.org/10.31349/RevMexFis.67.041001

1. Introduction

In recent years a very important technological interest in semiconductor alloys has been reserved in the literature for applications in the fields of optical devices [1,2]. Several authors have studied a wide range of materials to search for the desired parameters [3-6]. Thus, some kinds of semiconductors have been investigated theoretically, especially for the development and applications of mismatched alloys based on II-VI and III-V compounds. Due to the importance of the physical properties of such materials, works were motivated in III-V and II-VI [7-9] alloys for the development of new devices operating in the wide spectrum range. Particularly few authors indicate the wavelength region 1-2 μm [10-14] for optoelectronic devices in optical communication applications. Theoretically, different methods have been used for the calculation of the properties of semiconductor alloys. The full potential linear augmented plane wave method (FP-LAPW) within the density functional theory (DFT) has been used to compute the structural, electronic, and optical properties of several III-V and II-VI alloys. Thus, this method has recently been used for both ternary and quaternary alloys based on II-VI [15-17] and III-V [18,19] compounds. However, a major condition of materials for optoelectronic applications is the ability to adjust easily the band-gap to obtain the desired optical properties in order to ensure its matching with a given substrate. The quaternary (II-VI) alloys meet these requirements. Very recently, the structural and optoelectronic properties of $Zn_{1-x}Cd_xSe_yTe_{1-y}$ quaternary alloys [20] have been investigated using the density functional theory (DFT) based full-potential linearized augmented plane wave (LAPW) approach. Thus, the structural properties have been computed using the Perdew-Burke-Ernzerhof (PBE) generalized gradient approximation (GGA) scheme, while the optoelectronic properties have been calculated using both the modified Becke-Johnson (mBJ) and Engel-Vosko (EV-GGA) schemes. Hence the important interest in calculating the structural, electronic, and optical properties of $Zn_{1-x}Cd_xSe_yTe_{1-y}$ quaternary alloy using the (FP-LAPW) method within density functional theory (DFT) in order to collect much information, complete the previous works, and improve the knowledge of the field. In the rest of this article, we present the sections as follows: the computational method used in this paper will be described in Sec. 2 and our results will be reported and discussed in Sec. 3. Finally, as conclusions, a summary of the present work will be given in Sec. 4.

2. Computational method

In our work, we have computed the structural, electronic, and optical properties of $Zn_{1-x}Cd_xSe_yTe_{1-y}$ quaternary alloys, using the Full Potential Linearized Augmented Plane Wave (FP-LAPW) method [21] within the framework of the Density Functional Theory (DFT) as implemented in the WIEN2K code [22]. The FP-LAPW method principle is based on dividing the space into non-overlapping muffin-tin

(MT) spheres around the atomic sites and an interstitial region (IR). Inside the MT spheres, the charge density and potential are expanded by spherical harmonic functions. In addition, in the IR region, the basis set consists of plane waves. For structural parameters, the exchange-correlation potential was performed using the Perdew-Burke-Ernzerhof Generalized Gradient Approximation (GGA-PBEsol) [23]. On the other hand, the Tran-Blaha modified Becke-Johnson (TB-mBJ) [24] in adding to the Local Density Approximation (LDA) [21] approaches have been used to calculate the electronic and optical properties of $Zn_{1-x}Cd_xSe_yTe_{1-y}$ quaternary alloys lattice-matched to ZnTe.

The quaternary alloy computed in this work is made of four binary compounds ZnSe, ZnTe, CdSe, CdTe. For these binary alloys, the normal structure, zinc blende (ZB), is adopted. However, in our simulation, the plane wave cut-off was used with the condition $R_{MT}.K_{\max} = 8$, where R_{MT} is the smallest muffin-tin sphere radius and $K_{\max}$ is the plane wave cut-off. We have chosen the muffin-tin radius (MT) as R_{MT}(Zn)= 2.2, R_{MT}(Cd)= 2.4, R_{MT}(Se)= 2.3 and R_{MT}(Te)= 2.6 atomic units (a.u). The Fourier expanded charge density was truncated at $G_{\max} = 12(Ryd)^{1/2}$. For the wave function expansion inside the atomic spheres the maximum l value was confined to $l_{\max} = 10$. To dissociate core from valence states, the cut-off energy is set to $-6Ryd$. The self-consistent calculations are considered to be converged when the total energy of the system is stable within 0.0001 Ryd. A $2 \times 2 \times 2$ supercell with 64 atoms was used in order to compute the $Zn_{1-x}Cd_xSe_yTe_{1-y}$ quaternary alloys. The obtained simple cubic supercell to simulate the $Zn_{1-x}Cd_xSe_yTe_{1-y}$ quaternary alloys is made by 32 atoms of valency II (Zn,Cd) and 32 atoms of valency VI (Se,Te). A mesh of 50 special k-points was taken in the irreducible wedge of the Brillouin zone to calculate the structural and electronic properties. On the other hand the optical properties calculations were performed using 500 k-points. For the $Zn_{1-x}Cd_xSe_yTe_{1-y}$ alloy, the epitaxial layers can be deposited on substrates by the Metal-Organic Chemical Vapor Deposition method (MOCVD) [2]. Further, the Molecular Beam Epitaxy (MBE) method [2,25] can be used for lattice matching the epitaxial layer to the substrate. The electronic configurations Zn($_3$d^{10}4s^2), Cd(4d^{10}5s^2), Se(3d^{10}4s^{2}4p^4), Te(4d^{10}5s^{2}5p^4) were chosen as valence states. The crystal structure of $Zn_{0.500}Cd_{0.500}Se_{0.437}Te_{0.563}$ quaternary alloy is shown in Fig. 1.

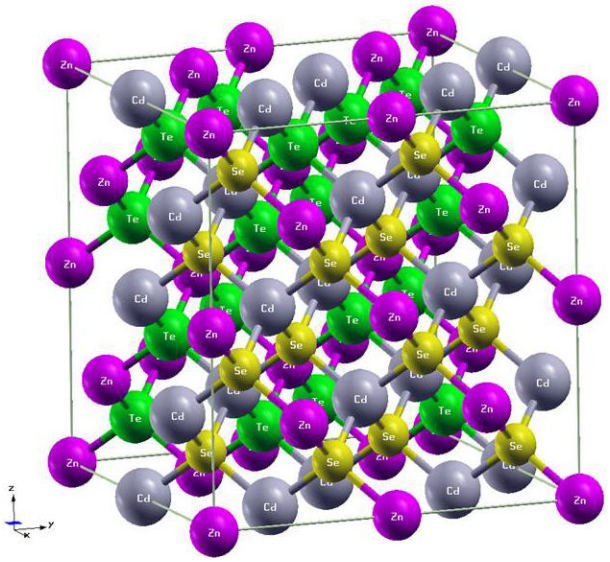

FIGURE 1. Crystal structure of $Zn_{0.500}Cd_{0.500}Se_{0.437}Te_{0.563}$ ($2 \times 2 \times 2$ supercell).

3. Results and discussions

3.1. Structural properties

Very interesting applications in semiconductor devices with desired band gaps were mentioned in the literature [26,27] on quaternary (II-VI) alloys having the general chemical formulas ($A_{1-x}B_xC_yD_{1-y}$) where AC, AD, BC, BD are the binary compounds and (x, y) are the concentrations. The aim of the present work is related to predicting the structural, electronic, and optical properties of $Zn_{1-x}Cd_xSe_yTe_{1-y}$ alloys with a number of Cd concentrations x ($0.125 \leq x \leq 0.875$). For the structural properties, the lattice parameter and bulk modulus were computed using the GGA-PBEsol approximation. In addition to the LDA approach, the recent (TB-mBJ) approach has been used to calculate the electronic and optical properties. The quaternary alloy $Zn_{1-x}Cd_xSe_yTe_{1-y}$ is bounded by four binary compounds ZnSe, ZnTe, CdSe, and CdTe. The normal structure of this binary is zinc-blende. Among 64 atom simple cubic structures, the ones that minimize the total energy with respect to the cell parameters and the atomic positions were searched. The simulated parameters have been computed as a function of cationic and anionic compositions (x, y), where x and y are the concentrations of Cd and Se elements, respectively. First, the structural properties of the binaries (ZnSe, ZnTe, CdSe, and CdTe) and the $Zn_{1-x}Cd_xSe_yTe_{1-y}$ quaternary alloys were computed by the GGA-PBEsol approximation. In order to compute the equilibrium lattice constants (a) and bulk modulus (B) for the $Zn_{1-x}Cd_xSe_yTe_{1-y}$ quaternary alloy, the total energy versus volume data have been calculated by fitting the total energy versus volume data into the Murnaghan's equation of states (EOS) [28]. The lattice constant of the quaternary $A_xB_{1-x}C_yD_{1-y}$ alloy is a function of the compositions (x, y) and can be approximated by the Vegard's law [2] given by the following relation:

$$a_Q = xya_{\mathrm{AC}} + x(1-y)a_{\mathrm{AD}} + (1-x)ya_{\mathrm{BC}} + (1-x)(1-y)a_{\mathrm{BD}}, \quad (1)$$

where a_{AC}, a_{AD}, a_{BC}, and a_{BD} correspond to the lattice constants for pure binaries AC, AD, BC, and BD, respectively.

TABLE I. Calculated lattice constant a(Å) and bulk modulus B(GPa) of $Zn_{1-x}Cd_xSe_yTe_{1-y}$ quaternary and their binaries by GGA-PBEsol method with experimental data and other theoretical calculations.

Compound	This work		Other works		Experiment	
	a(Å)	B(GPa)	a(Å)	B(GPa)	a(Å)	B(GPa)
ZnSe	5.647	65.32	5.650[a]	66.11[a]	5.669[b]	64.7[a]
CdSe	6.087	52.85	6.092[a]	52.76[a]	6.050[b]	53.0[a]
ZnTe	6.067	51.46	6.099[c]	51.59[c]	6.103[b]	50.9[c]
CdTe	6.495	45.71	6.420[d]	46.6[d]	6.481[b]	44.5[e]
$Zn_{0.875}Cd_{0.125}Se_{0.093}Te_{0.907}$	6.052	62.57	-	-	-	-
$Zn_{0.750}Cd_{0.250}Se_{0.218}Te_{0.782}$	6.064	62.07	-	-	-	-
$Zn_{0.625}Cd_{0.375}Se_{0.312}Te_{0.688}$	6.079	61.89	-	-	-	-
$Zn_{0.500}Cd_{0.500}Se_{0.437}Te_{0.563}$	6.083	61.35	-	-	-	-
$Zn_{0.375}Cd_{0.625}Se_{0.531}Te_{0.469}$	6.094	61.02	-	-	-	-
$Zn_{0.250}Cd_{0.750}Se_{0.656}Te_{0.344}$	6.103	61.60	-	-	-	-
$Zn_{0.125}Cd_{0.875}Se_{0.750}Te_{0.250}$	6.111	61.91	-	-	-	-

[a][17], [b][2], [c][15], [d][29], [e][30].

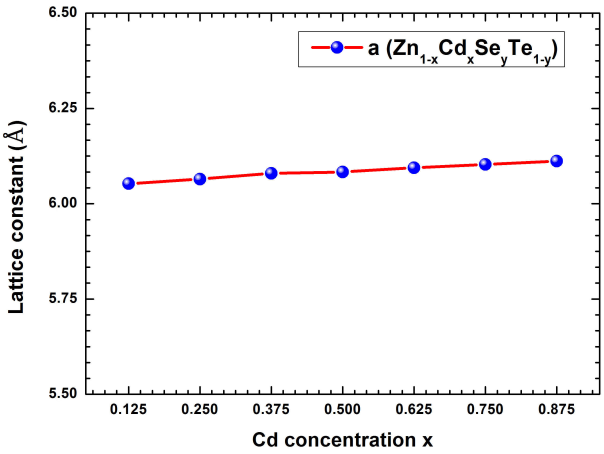

FIGURE 2. Calculated lattice constant as a function of the Cd concentration x in the $Zn_{1-x}Cd_xSe_yTe_{1-y}$ quaternary alloys matched to ZnTe with GGA-PBEsol method.

By using Eq. (1), the lattice constant for the $Zn_{1-x}Cd_xSe_yTe_{1-y}$ quaternary alloy can be deduced according to the following expression:

$$\begin{aligned} a_{Zn_{1-x}Cd_xSe_yTe_{1-y}} &= xya_{CdSe} \\ &+ x(1-y)a_{CdTe} + (1-x)a_{ZnSe} \\ &+ (1-x)(1-y)a_{ZnTe}, \end{aligned} \tag{2}$$

where the binaries AC, AD, BC, and BD are CdSe, CdTe, ZnSe, and ZnTe, respectively. The lattice-matching conditions are respected by putting $a(Zn_{1-x}Cd_xSe_yTe_{1-y})$ equal to a_{ZnTe} . Thus, using the respective experimental lattice constants of the binary compounds ($a_{CdSe} = 6.050$ Å), ($a_{CdTe} = 6.481$ Å), ($a_{ZnSe} = 5.669$ Å) and ($a_{ZnTe} = 6.1037$ Å), the corresponding concentrations for lattice matched of $Zn_{1-x}Cd_xSe_yTe_{1-y}$ quaternary alloy can be obtained by the relation (3) below with different concentrations $x(0.125 \leq x \leq 0.875)$.

$$y = \frac{0.377x}{0.4347 - 0.0037x}. \tag{3}$$

We have adopted $Zn_{1-x}Cd_xSe_yTe_{1-y}$ alloy lattice-matched to ZnTe with some selected concentrations $(4/32 \leq x \leq 24/32)$. We have considered different concentrations along the line of lattice matching to ZnTe by assigning to the pair (x, y), the respective compositions (4/32;3/32), (8/32;7/32), (12/32;10/32), (16/32;14/32), (20/32;17/32), (24/32;21/32) and (28/32;24/32). Using the GGA-PBEsol method, the lattice constant and bulk modulus of the binaries (CdSe, CdTe, ZnSe, ZnTe), and the quaternary alloy $Zn_{1-x}Cd_xSe_yTe_{1-y}$ were calculated for various Cd concentration (x) and exhibited in Table I.

To the best of our knowledge, there is no theoretical simulation based on the FP-LAPW method, and no experimental values of the structural properties of $Zn_{1-x}Cd_xSe_yTe_{1-y}$ alloy for these concentrations have been presented up to now. Hence our calculations can be used to cover the lack of data for the studied alloy. It is seen from Table I that the calculated lattice constants of $Zn_{1-x}Cd_xSe_yTe_{1-y}$ are also in good agreement with the experimental value of the ZnTe lattice constant. The variation of lattice parameter versus Cd concentration is found to be almost constant (around 6.084 Å). Figure 2 shows the calculated lattice constant as a function of the Cd concentration x $(0.125 \leq x \leq 0.875)$. A marginal deviation of the lattice constant from Vegard's law can be observed. From Fig. 2, we can notice that at given Se concentration, the lattice constant increases almost linearly with increasing Cd concentration. The optimized variation of the lattice constants $a(x)$ was fitted by the quadratic function

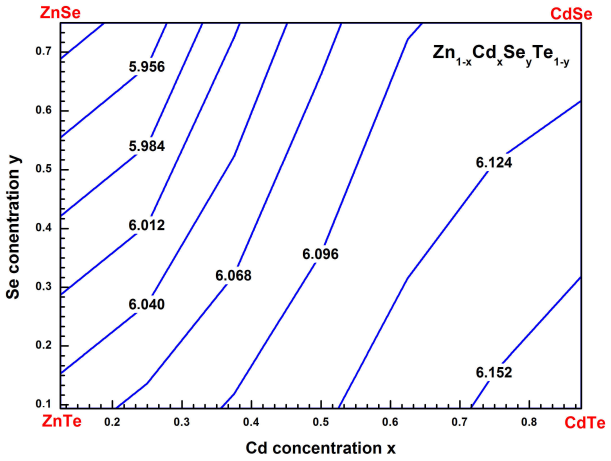

FIGURE 3. Contour lines of predicted lattice constant for $Zn_{1-x}Cd_xSe_yTe_{1-y}$ quaternary alloys matched to ZnTe with GGA-PBEsol method.

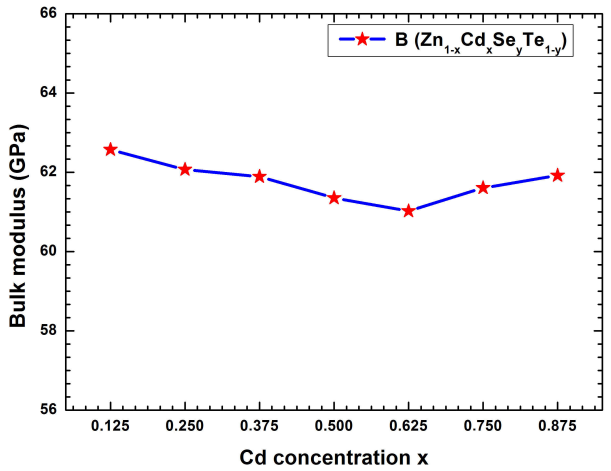

FIGURE 4. Calculated bulk modulus as a function of the Cd concentration x in the $Zn_{1-x}Cd_xSe_yTe_{1-y}$ quaternary alloys matched to ZnTe with GGA-PBEsol method.

to calculate the total bowing parameter (b). Thus, we have obtained the following relation:

$$a^{\text{GGA - PBEsol}}_{Zn_{1-x}Cd_xSe_yTe_{1-y}} = 6.0405 + 0.1042x - 0.0272x^2. \quad (4)$$

By referring to relation (4), we can observe a negligible bowing parameter ($b = -0.0272$ eV) corresponding to the quadratic term of the above equation. The contour lines of the lattice constants for $Zn_{1-x}Cd_xSe_yTe_{1-y}$ alloy as a function of Cd and Se compositions were simulated with the GGA-PBEsol approach and exhibited in Fig. 3. From this figure, it is observed that the lattice parameter of the quaternary alloy increases with increasing Cd concentration. The variation of the bulk modulus (B) versus Cd concentration (x) for the quaternary alloy $Zn_{1-x}Cd_xSe_yTe_{1-y}$ is reported in Table I and is shown in Fig. 4. It is seen to be almost constant. This result is in agreement with the well-known relationship between B and the lattice constant (B_α/V_0) [31], where V_0 is the unit cell volume.

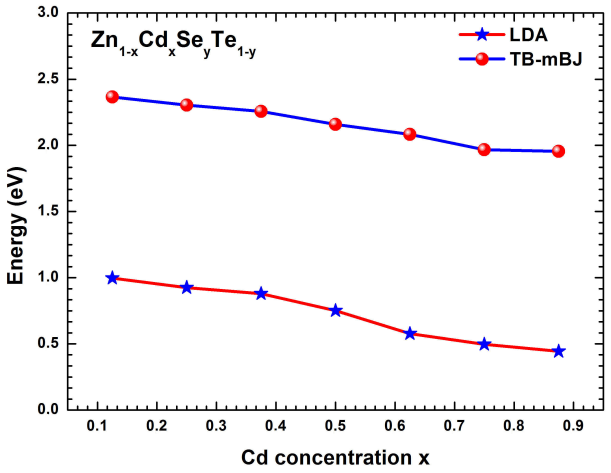

FIGURE 5. Bandgap energies Eg versus the concentration x for the $Zn_{1-x}Cd_xSe_yTe_{1-y}$ lattice-matched to ZnTe.

3.2. Electronic properties

This part is devoted to calculations of electronic band structure for $Zn_{1-x}Cd_xSe_yTe_{1-y}$ quaternary alloy without relaxation using the local density approximation (LDA) [32] and the Tran-Blaha modified Becker-Johnson (TB-mBJ) [24] approaches. This simulation was performed along the high symmetry lines of the first Brillouin zone, where the maximum of the valence band was fixed as the energy level reference. Table II exhibits the calculated energy band gaps (Eg) for the $Zn_{1-x}Cd_xSe_yTe_{1-y}$ quaternary alloy using LDA and TB-mBJ schemes for various Cd concentration x ($0.125 \leq x \leq 0.875$). To the best of our knowledge, there are no earlier studies of the bandgap for $Zn_{1-x}Cd_xSe_yTe_{1-y}$ alloys with these concentrations; hence our calculations can be used to cover the lack of data for the studied alloys. Figure 5 shows the variation of bandgap energies Eg versus the concentration x for $Zn_{1-x}Cd_xSe_yTe_{1-y}$ lattice-matched to ZnTe, calculated via two schemes (LDA and TB-mBJ). We remark that the variation of the bandgap energies is almost linear with a

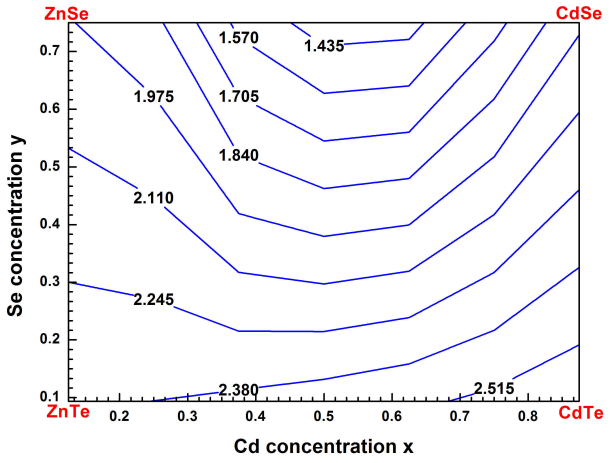

FIGURE 6. Energy band gap contour lines for $Zn_{1-x}Cd_xSe_yTe_{1-y}$ quaternary alloys matched to ZnTe with TB-mBJ method.

TABLE II. Calculated lattice constant a(Å) and bulk modulus B(GPa) of $Zn_{1-x}Cd_xSe_yTe_{1-y}$ quaternary and their binaries by GGA-PBEsol method with experimental data and other theoretical calculations.

Compound	This work		Other works		Experiment
	LDA	TB-mBJ	LDA	TB-mBJ	
ZnSe	1.102	2.443	1.060[a]	2.761[a]	2.721[d]
CdSe	0.397	1.849	0.316[a]	1.935[a]	1.675[d]
ZnTe	0.941	2.21	1.101[b]	1.83[b]	2.27[d]
CdTe	0.286	1.56	0.623[c]	-	1.51[d]
$Zn_{0.875}Cd_{0.125}Se_{0.093}Te_{0.907}$	0.997	2.365	-	-	-
$Zn_{0.750}Cd_{0.250}Se_{0.218}Te_{0.782}$	0.925	2.304	-	-	-
$Zn_{0.625}Cd_{0.375}Se_{0.312}Te_{0.688}$	0.879	2.257	-	-	-
$Zn_{0.500}Cd_{0.500}Se_{0.437}Te_{0.563}$	0.751	2.158	-	-	-
$Zn_{0.375}Cd_{0.625}Se_{0.531}Te_{0.469}$	0.577	2.083	-	-	-
$Zn_{0.250}Cd_{0.750}Se_{0.656}Te_{0.344}$	0.496	1.967	-	-	-
$Zn_{0.125}Cd_{0.875}Se_{0.750}Te_{0.250}$	0.433	1.854	-	-	-

[a][17], [b][15], [c][29], [d][2].

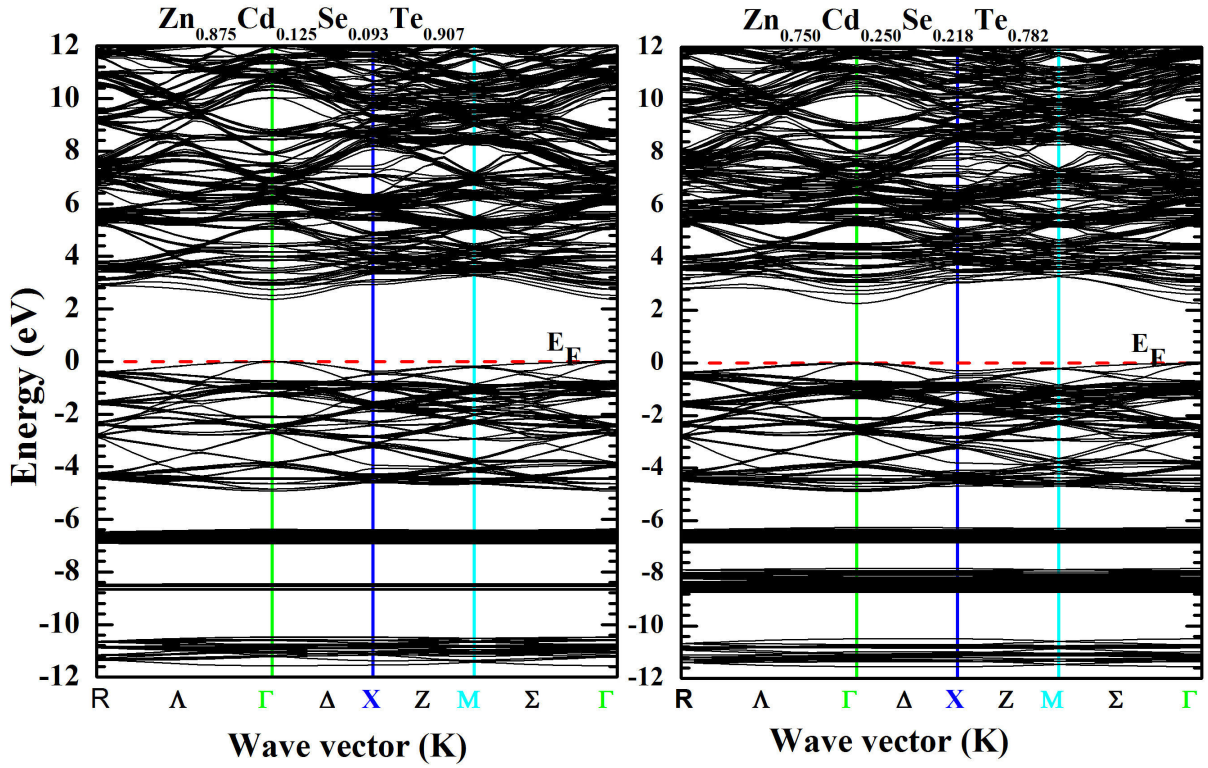

FIGURE 7. Band structure calculated for $Zn_{0.875}Cd_{0.125}Se_{0.093}Te_{0.907}$ and $Zn_{0.750}Cd_{0.250}Se_{0.218}Te_{0.782}$ with TB-mBJ method.

slight decrease of the curves with increasing Cd concentration (x). A fitting operation to curves presented in Fig. 5 was performed to determine the dependence of the energy band gaps (Eg) versus the composition of the cadmium (x) for the $Zn_{1-x}Cd_xSe_yTe_{1-y}$ lattice matched to ZnTe. Hence, we have obtained the following relations:

$$Eg^{LDA}(x) = 1.1029 - 0.6757x - 0.1310x^2, \quad (5)$$

$$Eg^{TB-mBJ}(x) = 2.4443 - 0.5489x - 0.0456x^2. \quad (6)$$

From these equations, we can determine for a given composition (x) the related band gap (Eg) in the $Zn_{1-x}Cd_xSe_yTe_{1-y}$ alloy lattice matched to ZnTe. Thus, for

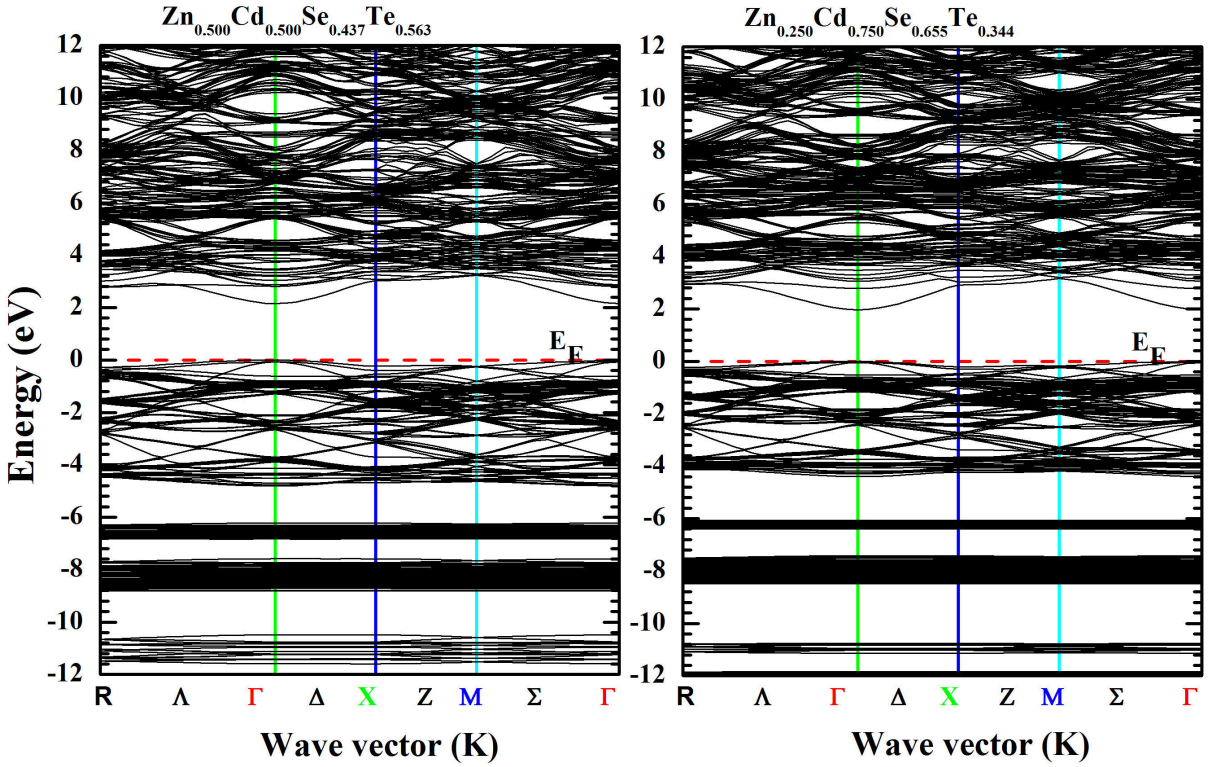

FIGURE 8. Band structure calculated for $Zn_{0.500}Cd_{0.500}Se_{0.437}Te_{0.563}$ and $Zn_{0.250}Cd_{0.750}Se_{0.656}Te_{0.344}$ with TB-mBJ method.

the studied structure, we got the values (-0.1310 eV) and (-0.0456 eV) corresponding to the bowing parameter (b) for LDA and TB-mBJ schemes, respectively. As presented in Fig. 5, one notes the slight decreasing of the bandgap of $Zn_{1-x}Cd_xSe_yTe_{1-y}$ alloy with the increase of the Cd concentration (x). The computed TB-mBJ energy bandgap contour lines of $Zn_{1-x}Cd_xSe_yTe_{1-y}$ alloy versus Cd and Se concentrations are exhibited in Fig. 6. The contour lines allow the reading of values from the curve. The electronic band structures were computed for $Zn_{1-x}Cd_xSe_yTe_{1-y}$ quaternary alloy with the predicted lattice constant using the TB-mBJ method. The corresponding results are shown in Figs. 7 and 8 for both quaternaries ($Zn_{0.875}Cd_{0.125}Se_{0.093}Te_{0.907}$; $Zn_{0.750}Cd_{0.250}Se_{0.218}Te_{0.782}$) and ($Zn_{0.500}Cd_{0.500}Se_{0.437}Te_{0.563}$; $Zn_{0.250}Cd_{0.750}Se_{0.656}Te_{0.344}$) respectively. The calculations were performed along the high-symmetry lines of the first Brillouin zone, and the Fermi level has been set to zero. As shown in the figures cited above, the respective levels for the maximum valence band (VBmax) and minimum conduction band (CBmin) are located at Γ point. Therefore, we conclude that the $Zn_{1-x}Cd_xSe_yTe_{1-y}$ quaternary is a direct bandgap alloy for the studied concentrations and is intended for optoelectronic applications.

3.3. Optical properties

The rest of our work will be devoted to studying the optical properties of $Zn_{1-x}Cd_xSe_yTe_{1-y}$ quaternary alloy. The calculations were performed at the equilibrium lattice constant of $Zn_{1-x}Cd_xSe_yTe_{1-y}$ with x ($0.250 \leq x \leq 0.875$) using TB-mBJ approach. This method has an essential role in optical applications [33]. On the other hand, using the FP-LAPW method, Abt *et al.* [34] and Ambrosch-Draxl and Sofo [35] have detailed the procedure of optical properties calculation for semiconductor alloys. From the complex dielectric function dependent on the frequency $\varepsilon(\omega)$, several optical parameters of semiconductor materials can be deduced. The cited function is composed of two terms as follows:

$$\varepsilon(\omega) = \varepsilon_1(\omega) + i\varepsilon_2(\omega), \tag{7}$$

where $\varepsilon_1(\omega)$ and $\varepsilon_2(\omega)$ present the real and imaginary part of the dielectric function, respectively. The $\varepsilon_2(\omega)$ values are determined directly from the electronic structure calculation through the joint density of states and the maximum matrix elements between the occupied eigenstates [2,36-38]:

$$\varepsilon_2(\omega) = \left(\frac{4\pi^2 e^2}{m^2\omega^2}\right) \sum_{ij} \int \langle iMj\rangle^2 \times f_i(1-f_i)\delta(E_f - E_i - \omega)d^3k \tag{8}$$

where M, f_i, and ω are the dipole matrix, Fermi distribution function, and the frequency of the incident photon, respectively. Thus, knowing $\varepsilon_2(\omega)$, we can then calculate $\varepsilon_1(\omega)$ using the Kramers-Kroning [39]: relation expressed as:

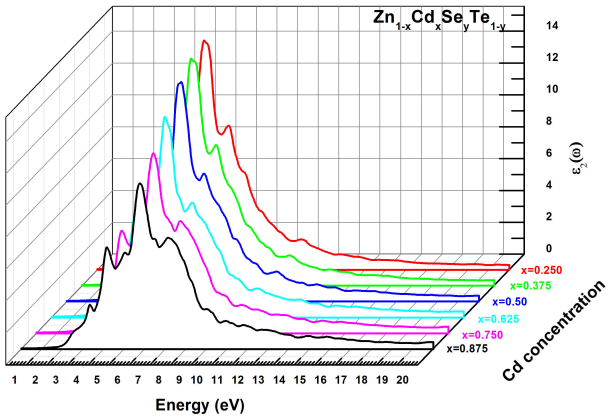

FIGURE 9. Imaginary part of the dielectric function $\varepsilon_2(\omega)$ for $Zn_{1-x}Cd_xSe_yTe_{1-y}$ alloys using TB-mBJ method.

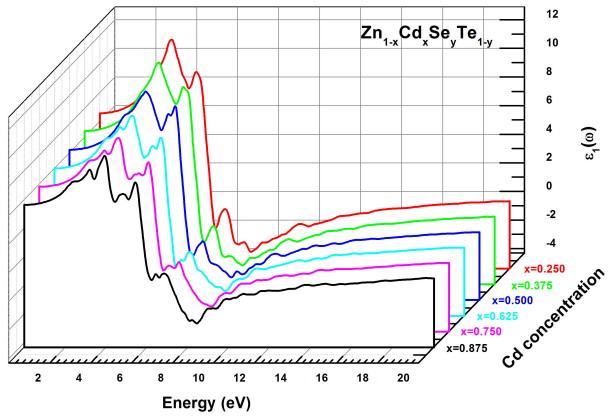

FIGURE 10. Real part of the dielectric function $\varepsilon_1(\omega)$ for $Zn_{1-x}Cd_xSe_yTe_{1-y}$ alloys using TB-mBJ method.

$$\varepsilon_1(\omega) = 1 + \frac{2}{\pi} p \int_0^{\infty} \frac{\omega' \cdot \varepsilon_2(\omega')}{\omega'^2 - \omega^2} d\omega'. \tag{9}$$

where p is the principal of the integral value. The knowledge of a dense mesh of eigenvectors [22] allows to determine the optical parameters. Thus, in our study, we have used 172k-points in the irreducible part of the Brillouin zone. The half-width Lorentzian broadening was set to 0.1 eV, and the simulated material structure has a cubic symmetry. Moreover, other interesting optical parameters related to the dielectric function can be calculated [40,41]. Among these parameters, we limit our study to the refractive index $n(\omega)$, the extinction coefficient $k(\omega)$, the absorption coefficient $\alpha(\omega)$ and the reflectivity $R(\omega)$, which are defined by the following relationships [2,42]:

$$n(\omega) = \left(\frac{(\sqrt{\varepsilon_1^2(\omega) + \varepsilon_2^2(\omega)}) + \varepsilon_1(\omega)}{2} \right)^{1/2}, \tag{10}$$

$$k(\omega) = \left(\frac{(\sqrt{\varepsilon_1^2(\omega) + \varepsilon_2^2(\omega)}) - \varepsilon_1(\omega)}{2} \right)^{1/2}, \tag{11}$$

$$R(\omega) = \frac{(n(\omega) - 1)^2 + k^2(\omega)}{(n(\omega) + 1)^2 + k^2(\omega)}, \tag{12}$$

$$\alpha(\omega) = \frac{4\pi}{\lambda} k(\omega), \tag{13}$$

where ω and λ present the angular frequency and the light in vacuum wavelength, respectively. In this work, the variations of the real and imaginary parts of dielectric functions $\varepsilon_1(\omega)$ and $\varepsilon_2(\omega)$, versus the incident photon energy were computed with TB-mBJ method for $Zn_{1-x}Cd_xSe_yTe_{1-y}$ with different concentrations $x(0.250 \leq x \leq 0.875)$. The low energy limit of the real part $\varepsilon_1(\omega)$ is defined as the static dielectric constant $\varepsilon_1(0)$. In Table III are summarized the calculated $\varepsilon_1(0)$ values and the peaks values in the dielectric function $\varepsilon_2(\omega)$ for the $Zn_{1-x}Cd_xSe_yTe_{1-y}$ quaternary alloy. In Figs. 9 and 10 are shown respectively, the variations of the real and imaginary parts of dielectric functions $\varepsilon_1(\omega)$ and $\varepsilon_2(\omega)$, versus the incident photon energy on the range of (0-20eV) for $Zn_{1-x}Cd_xSe_yTe_{1-y}$ with $x(0.250 \leq x \leq 0.875)$. The peak values ($E_1$,$E_2$,$E_3$) of the dielectric imaginary part function $\varepsilon_2(\omega)$ based on photon energy are derived from Fig. 9 and resumed in Table III. These energy peak values illustrate the electronic crossing of the valence band to the transmission band. Generally, we remark the same behavior of $\varepsilon_2(\omega)$ for both Cd concentrations. E_0 is defined as the threshold energy

TABLE III. Calculated critical points of the peaks (eV) in the dielectric function $\varepsilon_2(\omega)$ and the static optical parameter $\varepsilon_1(0)$ for $Zn_{1-x}Cd_xSe_yTe_{1-y}$ quaternary alloys with TB-mBJ method.

Compound	This work					Other work			Experiment		
	E_0	E_1	E_2	E_3	$\varepsilon_1(0)$	E_1	E_2	E_3	E_1	E_2	E_3
$Zn_{0.750}Cd_{0.250}Se_{0.218}Te_{0.782}$	2.237	4.293	5.231	6.400	6.564	-	-	-	-	-	-
$Zn_{0.625}Cd_{0.375}Se_{0.312}Te_{0.688}$	2.257	4.364	5.306	6.522	6.421	-	-	-	-	-	-
$Zn_{0.500}Cd_{0.500}Se_{0.437}Te_{0.563}$	2.150	4.395	5.580	6.706	6.204	-	-	-	-	-	-
$Zn_{0.375}Cd_{0.625}Se_{0.531}Te_{0.469}$	2.008	4.263	5.546	6.858	6.002	-	-	-	-	-	-
$Zn_{0.250}Cd_{0.750}Se_{0.656}Te_{0.344}$	1.967	4.179	5.715	7.040	5.799	-	-	-	-	-	-
$Zn_{0.125}Cd_{0.875}Se_{0.750}Te_{0.250}$	1.954	4.163	5.573	7.199	5.639	-	-	-	-	-	-

TABLE IV. Calculated refractive index (n) versus the concentration (x) for $Zn_{1-x}Cd_xSe_yTe_{1-y}$ quaternary alloys with TB-mBJ method.

Compound		This work	Other work	Experiment
		n	n	n
$Zn_{1-x}Cd_xSe_yTe_{1-y}$	x			
	0.250	2.562	-	-
	0.375	2.534	-	-
	0.500	2.490	-	-
	0.625	2.450	-	-
	0.750	2.408	-	-
	0.875	2.374	-	-

of the dielectric function and determines the direct optical transitions between the highest valence band (HVB) and the lowest conduction band (LCB) at Γ point. E_2 and E_3 peaks move to lower energies while E_2 peaks shift towards lower energies. On the other hand, E_1 and E_3 peak sizes decrease with the increase of Cd concentration while E_2 peak increases with increasing of x concentration. Referring to Table III, it is observed that the $\varepsilon_1(0)$ value decreases with increasing of Cd concentration for the $Zn_{1-x}Cd_xSe_yTe_{1-y}$ quaternary alloy. We also note from Fig. 10 that the real part $\varepsilon_1(\omega)$ increases for the photon energy values between 2 and 7 eV with two peaks E_0 and E_1, equal to 5 and 7 eV, respectively. Then $\varepsilon_1(\omega)$ decreases sharply with the energy increasing from the value of 7 eV and reaches its minimum for the energy value of 10 eV.

The refractive index (n) was computed at the equilibrium lattice constant. The results performed with the TB-mBJ method are exhibited in Table IV. The spectral curves of the refractive index $n(\omega)$ for $Zn_{1-x}Cd_xSe_yTe_{1-y}$ alloy are presented in Fig. 11 and show that the critical points of $n(\omega)$ change with the variation of the direct bandgap value (E_g). The refractive index $n(\omega)$ increases with E_g between 0 and 4.0 eV, then reaches its maximum value in the energy range ($4.5-6$ eV).

For energy values between 6 and 10 eV, $n(\omega)$ decreases progressively. The minimum value of $n(\omega)$ is obtained for $E_g > 10$ eV. Also, the variation of the refractive index (n) versus the concentration (x) was studied and presented in Fig. 12, which indicates that (n) varies linearly and decreases with increasing Cd concentration (x). By extrapolating the calculated refractive index $n(x)$ to a polynomial equation, a bowing parameter ($b = -0.025$ eV) was obtained, as shown in the following relation:

$$n^{\text{TB-mBJ}}_{Zn_{1-x}Cd_xSe_yTe_{1-y}}(x) = 2.637 - 0.282x - 0.025x^2. \quad (14)$$

As described in previous expressions of optical properties showing the relationships between the dielectric constant, the extinction, and absorption coefficient, hence we have simulated this last parameter $\alpha(\omega)$ for the $Zn_{1-x}Cd_xSe_yTe_{1-y}$ quaternary alloy. In semiconductor materials, the absorption phenomena manifest itself when the photon energy of the incident beam is higher than E_g ($h\gamma > Eg$), leading the electrons excitation from the valence band (VB) to the conduction (CB). The calculated absorption coefficient $\alpha(\omega)$ for $Zn_{1-x}Cd_xSe_yTe_{1-y}$ quaternary alloy is plotted in Fig. 13. Thus, we remark a sharp variation of $\alpha(\omega)$ occurring approximatively in the photon energy range ($2-10$ eV). More specif-

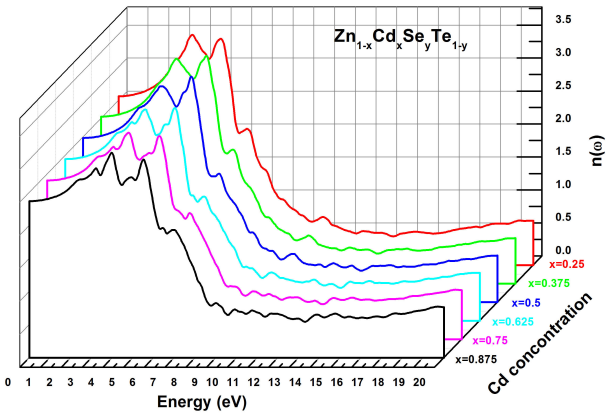

FIGURE 11. Calculated refractive index $n(\omega)$ for $Zn_{1-x}Cd_xSe_yTe_{1-y}$ quaternary alloys using TB-mBJ method.

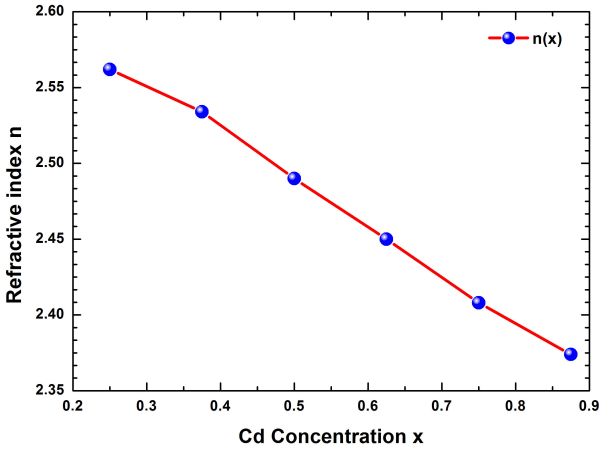

FIGURE 12. Refractive index (n) of $Zn_{1-x}Cd_xSe_yTe_{1-y}$ quaternary alloys versus the concentration (x) with TB-mBJ method.

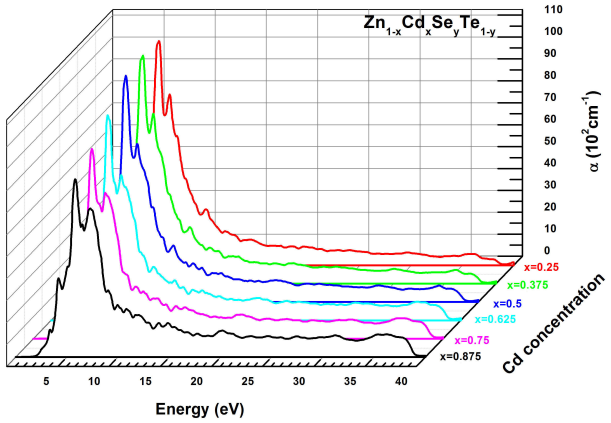

FIGURE 13. Calculated absorption coefficient $\alpha(\omega)$ for $Zn_{1-x}Cd_xSe_yTe_{1-y}$ quaternary alloys using TB-mBJ method.

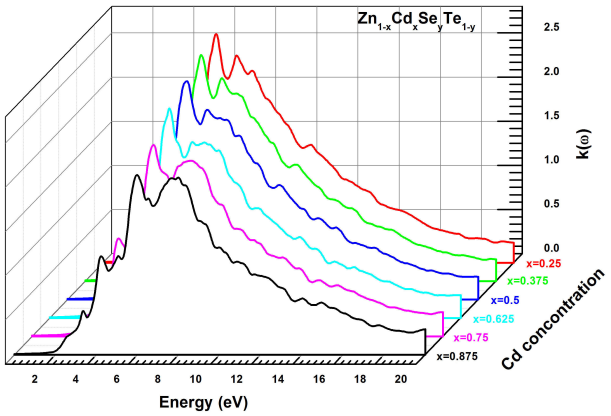

FIGURE 14. Calculated extinction coefficient $k(\omega)$ for $Zn_{1-x}Cd_xSe_yTe_{1-y}$ quaternary alloys using TB-mBJ method.

ically, in low energies ($2-7$ eV), the absorption coefficient increases rapidly and then decreases strongly for energies included in the interval ($7-10$ eV). The lowest values of $\alpha(\omega)$ were obtained for higher energies ($Eg > 15$ eV).

The extinction coefficient $k(\omega)$ was determined using the same method and conditions as the refractive index for $Zn_{1-x}Cd_xSe_yTe_{1-y}$ quaternary alloy. Figure 14 exhibits the curves of the extinction coefficient $k(\omega)$, which increases quickly in the energy range ($2-6.5$ eV) and decreases for ($Eg > 8.0$ eV). We note that the maximum values of $k(\omega)$ correspond to the minimum values of $\varepsilon_1(\omega)$ for the same energy interval. On the other hand, we observe that $k(\omega)$ is larger in the energy gap around ($6-10$ eV). This is an interesting criterion for the fluorescence phenomenon. The last parameter studied in this paper is the reflectivity $R(\omega)$ for $Zn_{1-x}Cd_xSe_yTe_{1-y}$ alloy that was simulated using the TB-mBJ method. The corresponding results are shown in Fig. 15, which indicates that the maximum reflectivity $R(\omega)$ occurs for photon energy values within a range of ($4.2-12.0$ eV). In addition, $R(\omega)$ declines rapidly for higher energy ($E > 15$ eV). According to the literature, the maximum reflectivity is related to the resonance plasmon that appears in the visible-ultraviolet area.

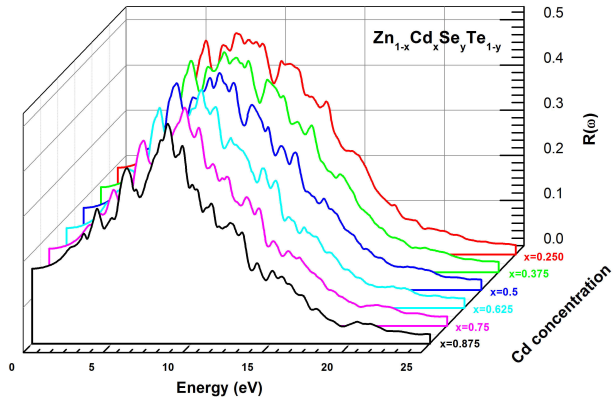

FIGURE 15. Calculated reflectivity $R(\omega)$ for $Zn_{1-x}Cd_xSe_yTe_{1-y}$ quaternary alloys using TB-mBJ method.

The referenced work [20] presents many similarities in objectives and methodologies to the present work. Both studied the same quaternary alloy using the Wien2k code with PBE and the approximation mBJ. On the other hand, Vegard's law and the same principle were used to calculate the optical properties. In our work, an improved ($2\times2\times2$) model cell was chosen, and calculations were performed with PBEsol and the approximation TB-mBJ rather than ($1\times1\times1$) model cell, PBE and mBJ method used in [20], respectively. This work uses another range x ($0.125 \leq x \leq 0.875$) for equating the parameter to ZnTe. Globally, the quaternary alloys studied in both works present the same behavior. Our results and those of reference [20] are consistent with each other and have similarities in particular as regards the energy gap $Eg(x)$, real and imaginary part of the dielectric function $\varepsilon_1(\omega)$ and $\varepsilon_2(\omega)$, and the refractive index $n(\omega)$. Finally, the results obtained in the present paper confirm that ZnTe is a suitable substrate for the growth of zincblende $Zn_{1-x}Cd_xSe_yTe_{1-y}$ quaternary alloys as suggested in [20].

4. Conclusion

To summarize, we have performed the FP-LAPW method within DFT to study the structural, electronic, and optical properties of $Zn_{1-x}Cd_xSe_yTe_{1-y}$ quaternary alloys matched to ZnTe as a function of the Cd composition. For the binary compounds, the computed structural parameters using the GGA-PBEsol approach, as well as the calculated energy gap with LDA and TB-mBJ methods, are found to be in good agreement with experimental data and other previous works. The variation of lattice constant, bulk modulus, and energy gap for $Zn_{1-x}Cd_xSe_yTe_{1-y}$ quaternary alloys on the concentration $x(0.125 \leq x \leq 0.875)$ are seen to be almost linear. It should be noted that the direct nature of the bandgap in the binary compounds is well preserved in the studied quaternary alloys. The effects of the Cd concentration and photon energy on the optical properties of $Zn_{1-x}Cd_xSe_yTe_{1-y}$ quaternary alloys were also predicted. Specifically, the refractive index (n) varies linearly and decreases with increasing of Cd concentration. On the other

hand, $n(\omega)$ change with the variation of the direct bandgap value (Eg) and reaches its maximum value in the energy range ($4.5 - 6.0$ eV). In addition, the $Zn_{1-x}Cd_xSe_yTe_{1-y}$ quaternary alloys show strong absorption in the energy range ($5.0 - 10.0$ eV). Moreover, the extinction coefficient $k(\omega)$ is larger in the energy gap ($6.0 - 10.0$ eV), which corresponds to the interval of the minimum value part of the dielectric function $\varepsilon_1(\omega)$. The obtained results regarding the studied properties of the $Zn_{1-x}Cd_xSe_yTe_{1-y}$ quaternary alloys are found to be reasonable and show that related quaternary is a promising candidate for optoelectronic applications. Our computed results for the $Zn_{1-x}Cd_xSe_yTe_{1-y}$ quaternary alloys should be expected as a reference for future works due to the lack of experimental and theoretical data using the FP-LAPW calculations for the quaternary of interest.

Acknowledgments

The authors are thankful to the entire research team of the laboratory "*Applied Materials Laboratory (AML), Djillali Liabes University, Sidi Bel Abbes, Algeria*". This work was supported by the Directorate General for Scientific Research and Technological Development (DGRSDT) of Algeria.

1. S. Fujita, Wide-bandgap semiconductor materials: For their full bloom, *Jpn. J. Appl. Phys.* **54** (2015) 030101, http://dx.doi.org/10.7567/JJAP.54.030101.
2. S. Adachi, *Properties of semiconductor alloys: Group IV, III-V and II-VI semiconductors*, John Wiley & Sons Ltd, New York, (2009).
3. J. Van Vetchen, T. Bergstresser, Electronic structures of semiconductor alloys, *Phys. Rev. B* **1** (1970) 3351, https://doi.org/10.1103/PhysRevB.1.3351.
4. R. Hill, Energy-gap variations in semiconductor alloys, *J. Phys. C: Solid St. Phys.* **7** (1974) 521, https://doi.org/10.1088/0022-3719/7/3/009.
5. M. Jaros, Electronic properties of semiconductor alloy systems, *Rep. Prog. Phys.* **48** (1985) 1091, https://doi.org/10.1088/0034-4885/48/8/001.
6. F. Aymerich, Pseudopotential band structure of $Al_{1-x-y}Ga_xIn_yAs$, *Phys. Rev. B* **26** (1982) 1968, https://doi.org/10.1103/PhysRevB.26.1968.
7. M. Afzaal, and P. O'Brien, Recent developments in II-VI and III-V semiconductors and their applications in solar cells, *J. Mater. Chem.* **16** (2006) 1597, https://doi.org/10.1039/B512182E.
8. M. Hadjab, S. Berrah, H. Abid, M. I. Ziane, H. Bennacer and A.H. Reshak, First-principles investigation of the optical properties for rocksalt mixed metal oxide $Mg_xZn_{1-x}O$, *Mater. Chem. Phys*. **182** (2016) 182, https://doi.org/10.1016/j.matchemphys.2016.07.021.
9. N. Kobayashi and Y. Horikoshi, Liquid Phase Epitaxial Growth of $InAs_{1-x-y}P_xSb_y$ on InAs Substrate, *Jpn. J. Appl. Phys*. **20** (1981) 2301, https://doi.org/10.1143/JJAP.20.2301.
10. Y. Furukawa, Application of InGaAsP and AlGaAsSb for Optical Fiber Transmission, *Jpn. J. Appl. Phys*. **29** (1980) 295, https://doi.org/10.7567/JJAPS.19S3.295.
11. S. Adachi, Band gaps and refractive indices of AlGaAsSb, GaInAsSb, and InPAsSb: Key properties for a variety of the 2-4 μm optoelectronic device applications, *J. Appl. Phys*. **61** (1987) 4869, https://doi.org/10.1063/1.338352.
12. T.H. Chiu, J.L. Zyskind, and W.T. Tsang, Molecular Beam Epitaxial Growth of InGaAsSb on (100) GaSb with emission wavelength 1.2 to 2.5 μm range, *J.E.M* **16** (1987) 57, https://doi.org/10.1007/BF02667791.
13. D.K. Ghosh and L.K. Samanta, Refractive indices of some narrow and wide band materials, *Infrared Physics* **26** (1986) 335, https://doi.org/10.1016/0020-0891(86)90012-6.
14. A. Boumaza et al., First principles calculations of structural, electronic and optical properties of $Zn_{1-x}Be_xSe_yTe_{1-y}$ quaternary alloys, *Com. Mat. Sci*. **87** (2014) 202, http://dx.doi.org/10.1016/j.commatsci.2014.02.028.
15. Naeemullah, R. Khenata, G. Murtaza, and S. Bin Omran, Direct band gap nature and optical response of $Be_xMg_yZn_{1-(x+y)}Se$, *Mod. Phys. Lett. B* **30** (2016) 1650007, https://doi.org/10.1142/S021798491650007X.
16. H. Slimani, H. Abid, and M. Benchehima, Prediction of optoelectronic properties for $Be_xZn_yCd_{1-x-y}Se$ quaternary alloys: First-principles study, *Optik* **198** (2019) 163288, https://doi.org/10.1016/j.ijleo.2019.163288.
17. M. Benchehima and H. Abid, Electronic and optical properties of $Al_xGa_yIn_{1-x-y}$ As quaternary alloys with and without relaxation lattice matched to lnP for applications: First-principles study, *Optik* **127** (2016) 6541, http://dx.doi.org/10.1016/j.ijleo.2016.04.092.
18. A. Assali, M. Bouslama, A.H. Reshak, S. Zerroug, and H. Abid, Electronic structure and optical properties of dilute boron-bismide quaternary alloys $B_xGa_{1-x}As_{1-y}Bi_y$/GaAs for infrared Optoelectronic Devices, *Optik* **135** (2017) 57, http://dx.doi.org/doi:10.1016/j.ijleo.2017.01.059.
19. M. Berber, N. Bouzouira, M. Mebrek, A. Boudali, H. Abid, and H. Moujri, Structural, electronic, and optical properties of quaternary alloys $Al_{0.50}Ga_{0.50}N_xSb_{1-x}$: a first-principles study, *Rev. Mex. Fis.* **66** (2020) 790, https://doi.org/10.31349/RevMexFis.66.790.
20. S. Chanda, D. Ghosh, B. Debnath, M. Debbarma, R. Bhattacharjee, and S. Chattopadhyaya, Calculations of the structural and optoelectronic properties of cubic $Cd_xZn_{1-x}Se_yTe_{1-y}$ semiconductor quaternary alloys using the DFT-based FP-LAPW approach, *J. Comput. Electron* **19** (2020) 1, https://doi.org/10.1007/s10825-019-01409-0.

21. W. Kohn, and L. J. Sham, Self-Consistent Equations Including Exchange and Correlation Effects, *Phys. Rev*. **140** (1965) A1133, https://doi.org/10.1103/PhysRev.140.A1133.

22. P. Blaha, K. Schwarz, K.G.H. Madsen, D. Kvasnicka, and J. Luitz, *WIEN2K:* An Augmented Plane Wave + Local Orbitals Program for Calculating Crystal Properties, Austria, 2001.

23. J. P. Perdew *et al*., Restoring the Density-Gradient Expansion for Exchange in Solids and Surfaces, *Phys. Rev. Lett.* **100** (2008) 136406, https://doi.org/10.1103/PhysRevLett.100.136406.

24. F. Tran and P. Blaha, Accurate Band Gaps of Semiconductors and Insulators with a Semilocal Exchange-Correlation Potential, *Phys. Rev. Lett.* **102** (2009) 226401, https://doi.org/10.1103/PhysRevLett.102.226401.

25. J. Davies, A. Marshall, M. Scott, and R. Griffiths, Structural and optical properties of GaAlInAs lattice matched to InP grown by low-pressure metalorganic vapor phase epitaxy, *Appl. Phys. Lett*. **53** (1988) 276, https://doi.org/10.1063/1.100593.

26. J. Orton, and C. Foxon, Group III nitride semiconductors for short wavelength light emitting devices, *Rep. Prog. Phys.* **61** (1998) 1, https://doi.org/10.1088/0034-4885/61/1/001.

27. C.I.H. Ashby *et al.*, Low-dislocation-density GaN from a single growth on a textured substrate, *Appl. Phys. Lett.* **77** (2000) 3233, https://doi.org/10.1063/1.1325394.

28. F. Murnaghan, The Compressibility of Media under Extreme Pressures, *Proc. Natl. Acad. Sci USA* **30** (1944) 244, https://doi.org/10.1073/pnas.30.9.244.

29. W. Zeng, Q.J. Liu, and Z.T. Liu, First-Principles Local Density Plus Virtual Crystal Approximations Study of HgCdTe, W. *J. Appl. Phys*. **1** (2016) 26, https://doi.org/10.11648/j.wjap.20160101.14.

30. X. Chen, X. Hua, J. Hu, J. M. Langlois, and W. A. Goddard III, Band structures of II-VI semiconductors using Gaussian basis functions with separable ab initio pseudopotentials: Application to prediction of band offsets, *Phy. Rev. B* **53** (1996) 1377, https://doi.org/10.1103/PhysRevB.53.1377.

31. M.L. Cohen, Calculation of bulk moduli of diamond and zinc-blende solids, *Phys. Rev. B* **32** (1985) 7988, https://doi.org/10.1103/PhysRevB.32.7988.

32. B.R. Bennet, R. Magno, J.B. Boos, W. Kruppa, and M.G. Ancona, Antimonide-based compound semiconductors for electronic devices: *A review, Solid-State Electronics* **49** (2005) 1875, https://doi.org/10.1016/j.sse.2005.09.008.

33. Y. Yan, Q. Wang, W. Shu, Z. Jia, X. Ren, X. Zhang, and Y. Huang, First-principle study of the electronic and optical properties of BInGaAs quaternary alloy lattice-matched to GaAs, *Phys. B Condens. Matter* **407** (2012) 4570, https://doi.org/10.1016/j.physb.2012.08.021.

34. R. Abt, C. Ambrosch-Draxl, and P. Knoll, Optical response of high temperature superconductors by full potential LAPW band structure calculations, *Phys. B Condens. Matter* **194** (1994) 1451, https://doi.org/10.1016/0921-4526(94)91225-4.

35. C. Ambrosch-Draxl, and J.O. Sofo, Linear optical properties of solids within the full-potential linearized augmented planewave method, *Comput. Phys. Commun*. **175** (2006) 1, https://doi.org/10.1016/j.cpc.2006.03.005.

36. A. Zunger, S.H. Wei, L. Ferreira, and J.E. Bernard, Special quasirandom structures, *Phys. Rev. Lett*. **65** (1990) 353, https://doi.org/10.1103/PhysRevLett.65.353.

37. M. Benchehima, H. Abid, A. Sadoun, and A.C. Chaouche, Optoelectronic properties of aluminum bismuth antimony ternary alloys for optical telecommunication applications: First principles calculation, *Com. Mat. Sci.* **155** (2018) 224, https://doi.org/10.1016/j.commatsci.2018.08.050.

38. A. Gazhulina and M. Marychev, Structural, electronic and nonlinear optical properties of B3 and B20 compounds: A first-principles investigation within the LDA, GGA and modified Becke-Johnson exchange potential plus LDA, *J. All. Com.* **623** (2015) 413, https://doi.org/10.1016/j.jallcom.2014.11.028.

39. T. Ouahrani *et al*., Ab-initio study of the structural, linear and nonlinear optical properties of CdAl2Se4 defect-chalcopyrite, *J. Solid State Chem.* **183** (2010) 46, https://doi.org/10.1016/j.jssc.2009.09.034.

40. Z.Y. Jiao, S.H. Ma, and Y.L. Guo, Simulation of optical function for phosphide crystals following the DFT band structure calculations, *Comp. T. C.* **970** (2011) 79, https://doi.org/10.1016/j.comptc.2011.05.030.

41. N. Korozlu, K. Colakoglu, and E. Deligoz, Structural, electronic, elastic and optical properties of CdxZn1-xTe mixed crystals, *J. Phys. Condens. Matter* **21** (2009) 175406, https://doi.org/10.1088/0953-8984/21/17/175406.

42. F. Wooten, *Optical Properties of Solids*, Academic Press, New York (1972) 49.